AGU PUBLICATIONS

JGR

Journal of Geophysical Research: Oceans

RESEARCH ARTICLE

10.1002/2013JC009754

**Key Points:**
- Postbloom scenario can provide a high export of particulate organic carbon
- Enhanced carbon export can be driven by flux of particles <1.0 mm
- Fecal pellet fragments can be important for the downward carbon flux

**Correspondence to:**
I. Wiedmann,
Ingrid.wiedmann@uit.no

**Citation:**
Wiedmann, I., M. Reigstad, A. Sundfjord, and S. Basedow (2014), Potential drivers of sinking particle's size spectra and vertical flux of particulate organic carbon (POC): Turbulence, phytoplankton, and zooplankton, *J. Geophys. Res. Oceans*, *119*, 6900–6917, doi:10.1002/2013JC009754.

Received 20 DEC 2013
Accepted 18 SEP 2014
Accepted article online 22 SEP 2014
Published online 16 OCT 2014



# Potential drivers of sinking particle's size spectra and vertical flux of particulate organic carbon (POC): Turbulence, phytoplankton, and zooplankton

**Ingrid Wiedmann[1], Marit Reigstad[1], Arild Sundfjord[2], and Sünnje Basedow[3]**

[1]Department of Arctic and Marine Biology, UiT The Arctic University of Norway, Breivika, Tromsø, Norway, [2]Norwegian Polar Institute, Framsenteret, Tromsø, Norway, [3]University of Nordland, Bodø, Norway

**Abstract** Phytoplankton spring blooms in temperate and high-latitude shelf seas are commonly associated with an enhanced particulate organic carbon (POC) export of aggregates from the euphotic zone. In contrast, a postbloom situation is usually linked to a predominant POC retention, where small cells (<10 $\mu$m) and strong grazing pressure prevail. This study aimed to examine impacts of turbulence, phytoplankton, bloom stage, and zooplankton abundance on the sinking particles' size spectra and POC flux to improve the understanding of the downward flux mechanisms in the upper 100 m. We deployed sediment traps, partly modified with gel jars, at four depths along a stratification and phytoplankton bloom gradient in the Barents Sea, an Arctic shelf sea. The highest POC export (60 m: 923 mg C $m^{-2}$ $d^{-1}$) was found in deep-mixed, postbloom Atlantic influenced waters, despite the high grazer abundance (12,000 individuals $m^{-3}$). Particle size spectra indicated that this flux was dominated by particles of 0.05–1.00 mm equivalent spherical diameter ($ESD_{image}$) with a POC:volume ratio matching copepod fecal pellets. Large particles (0.5–2.8 mm $ESD_{image}$) dominated the flux at a stratified, late peak bloom station in Arctic Waters and a stratified, late bloom situation at the Polar Front, but with lower POC:volume ratio and POC flux (60 m: <823 mg C $m^{-2}$ $d^{-1}$). Accordingly, a high POC flux at the base of the euphotic zone is not necessarily driven by large phytoplankton aggregates, but can also occur during a postbloom situation in form of small fecal pellet fragments with high POC content.

## 1. Introduction

The export of particulate organic carbon (POC) in temperate and high-latitude shelf seas tends to fluctuate between (1) a strong carbon export, often associated with e.g., diatom blooms, and (2) a prevailing POC retention with small cells (<10 $\mu$m) and a major carbon recycling through the microbial loop [*Wassmann*, 1998; *Tamigneaux et al*., 1999]. Several studies indicate that a future warming and freshening of these seas will increase the importance of picoplankton [*Li et al*., 2009; *Morán et al*., 2010]. These investigations further propose that a change in community size structure may also alter the export and retention of POC in the water column. It is therefore important to focus on mechanisms and regulation of the vertical particle flux in contrasting phases, as this forms the basis for understanding consequences for the biological carbon pump in a future ocean.

An enhanced POC export is typically observed during a phytoplankton bloom [*Wassmann*, 1998]. A mismatch of intensely growing autotrophic algae and grazing by herbivore zooplankton causes first an accumulation of biomass in the euphotic zone, followed by an enhanced vertical POC flux to deeper layers. Phytoplankton can either sink in form of single cells (e.g., diatom resting spores) or as aggregates, formed by coagulation of sticky cells [*McCave*, 1984; *Smetacek*, 1985; *Alldredge*, 2001]. Zooplankton like copepods and krill contribute to the enhanced POC flux by grazing on small organic particles and producing large, fast-sinking fecal pellets [*McCave*, 1984; *Hamm et al*., 2001]. In contrast, a retention dominated system is usually linked to a postbloom situation [*Wassmann*, 1998]. Small primary producers and microzooplankton have been identified as central actors in this system [*Gifford et al*., 1995; *Møller et al*., 2006; *Hodal and Kristiansen*, 2008]. Due to the high carbon overturn, POC is here rather recycled in the pelagic food web than exported to depth.

Though the concept of a fluctuation between an export and retention dominated system is largely accepted, recent studies indicate that the link "large particles—export" (respectively, "small particles—retention") may not be representative for all pelagic systems at all times.

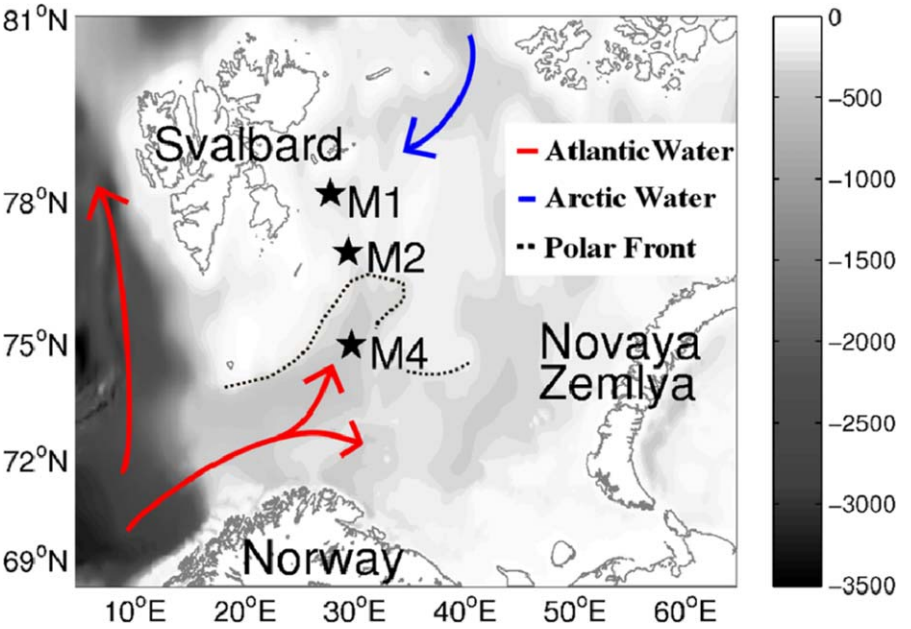


**Figure 1.** Sampling localities in the Barents Sea (bathymetry is given in gray shades, see color bar for depths in meters).

*McDonnell and Buesseler* [2010] suggested, for example, that small particles (equivalent spherical diameter, ESD: ~0.07–0.12 mm) can have a high sinking velocity, while medium-sized ones (ESD: ~0.12–0.50 mm) can sink slower. Ballasting effects have been suggested to play a major role for the downward flux [e.g., *Iversen et al*., 2010]. Further, it has also been put forward that cells of all sizes (even picoplankton) might contribute to the vertical carbon flux [*Richardson and Jackson*, 2007]. The present study was therefore designed to reconsider the link between particles sizes and intensity of the POC flux in the upper 100 m (zone of the strongest attenuation of sinking organic material) under contrasting hydrographical scenarios, spring bloom stages and grazer abundances by conducting sampling along a north-south transect in the Barents Sea (BS).

This Arctic shelf sea is surrounded by Norway, Svalbard, Franz Josef Land, and Novaya Zemlya (70–80°N; 15–60°E, Figure 1). It has a mean depth of 230 m and is a well-suited model area with contrasting water masses. Cold Arctic Water (<0°C, 34.3–34.8 salinity) enters the BS from the northeast, while the inflow of comparably warm and saline Atlantic Water (>3°C, >35.0 salinity) takes place at the southwestern opening, resulting in the formation of the Polar Front [*Loeng*, 1991; *Loeng et al*., 1997]. Sea ice is locally formed north of the Polar Front during winter and reaches its maximum extension in March to May. As ice-melting sets in, the marginal ice zone (MIZ) gradually retreats north and eastward, and the ice-free areas become stratified by a strong halocline. The resulting shallow mixed layer, the increased irradiance level, and the high nutrient concentrations facilitate phytoplankton blooms in the MIZ, resulting in an enhanced vertical carbon export before planktonic grazers become abundant [*Olli et al*., 2002]. Waters in the southwestern BS are permanently ice-free. Episodic strong winds from passing Polar Lows cause deep mixing (>30 m) until early summer [*Slagstad and Støle-Hansen*, 1991; *Ingvaldsen and Loeng*, 2009]. This partly counteracts the development of the spring bloom, but compared to the MIZ, the ice-free, Atlantic influenced waters have higher irradiance levels, promoting an early start of the primary production in the southwestern BS [*Wassmann et al*., 1991]. A peak bloom situation may thus still facilitate an enhanced POC export in the northern, Arctic influenced part of the BS, while a retention dominated, postbloom situation with an effective carbon grazing and recycling may already prevail in the southern, Atlantic part.

Sampling along a north-south transect in the BS thus gives insight into contrasting hydrographical situations and bloom scenarios within a short distance (late peak bloom in stratified waters versus postbloom in deep-mixed waters). We collected samples at representative stations in the Arctic part, the Polar Front, and the Atlantic part of the BS to quantify the hydrographical conditions, small-scale water shear, vertical diffusivity, and suspended biomass in the upper 100 m. Also, we determined the particle size spectra of sinking particles (>0.05 mm equivalent spherical diameter, $ESD_{image}$) collected by short-term sediment traps

**Table 1.** Station Identity (Incl. Ice Cover) and Sampling Schedule for Suspended Material[a]

| Station | Position | Date | Depth (m) | Ice Cover | Water Sampling (UTC) | Depth of Water Samples (m) |
|---|---|---|---|---|---|---|
| M1 | 78.0973°N, 28.1258°E | 22 Jun 2011 | 278 | Very open drift ice (30%) | 16:15 | 1, 5, 10, 20, 30, 31, 40, 50, 60, 90, 120, 200 |
| M2 | 76.9493°N, 29.7117°E | 24 Jun 2011 | 235 | Very open drift ice (20%) | 07:46 | 1, 5, 10, 20, 30, 40, 44, 50, 60, 90, 120, 200 |
| M4 | 74.9107°N, 30.0033°E | 27 Jun 2011 | 371 | Open water | 09:11 | 1, 5, 10, 20, 30, 40, 45, 50, 60, 90, 120, 200 |

[a]Water samples analyzed for particulate organic carbon (POC), total chlorophyll *a* >0.7 $\mu$m (Chl *a*) and Chl *a* >10 $\mu$m.

modified with gel jars (30, 40, 60, and 90 m). Based on these results, we addressed the questions (1) how do turbulence, prevailing phytoplankton taxa, and zooplankton abundance (used as approximation for the grazing pressure) influence the size spectra of the sinking particles and the vertical POC flux, and (2) if a high POC flux of material >0.7 $\mu$m is always associated with a bloom scenario characterized by large sinking particles (>0.5 mm) like diatom aggregates, marine snow, or fecal pellets.

## 2. Materials and Methods

Sampling was conducted on board the ice-enforced R/V "Helmer Hanssen" between 22 and 27 June 2011. We followed the 30°E longitude in the Barents Sea from north to south and sampled at three drift stations referred to as M1 (78°N), M2 (77°N), and M4 (75°N) (Figure 1 and Table 1). The stations were chosen as representative locations for well-stratified Arctic Water masses (M1), the Polar Front (M2), and deep-mixed Atlantic waters (M4) based on a northward high resolution CTD transect prior to station work (S. Basedow et al., unpublished data, 2012).

### 2.1. Hydrography, Small-Scale Current Shear, and Diffusivity

A standard sampling program on the hydrography was conducted at each of the three stations. Vertical profiles of temperature and salinity from surface to bottom were measured using a CTD-F (Sea-Bird 911*plus*). The CTD data were processed and bin averaged to 0.5 m using Sea-Bird's standard software package. Sea ice conditions were visually estimated using the scale of the Norwegian Meteorological Institute (11 categories from ice-free to fast ice) and recorded in the ship log.

Profiles of small-scale current shear and hydrography microstructure were measured with a loosely tethered turbulence dropsonde MSS-90L, equipped with a pair of PNS06 shear probes [*Prandke and Stips*, 1998]. The sets of three profiles were collected approximately every 4 h during each drift station. After processing of each set, mean profiles cover the depth range from 8 to >100 m. In this paper, the sets of microstructure profiles, which were taken closest in time to the deployment of each of the sediment traps with gel jars, are presented (Table 2). The microstructure data were processed as described in *Sundfjord et al.* [2007], but had a lower dissipation noise threshold due to use of a longer-bodied profiler and more optimal fall speed. Dissipation $\varepsilon$ (W kg$^{-1}$), vertical shear rate $S$ (s$^{-1}$), and diffusivity $K$ (m$^2$ s$^{-1}$) were calculated and bin averaged to 0.5 m:

$$\varepsilon = 7.5\nu \left(\partial u'/\partial z\right)^2 \quad (1)$$

**Table 2.** Sampling Schedule of the Sediment Traps (Partly Modified With Gel Jars, Denoted as "Gel Trap")[a] and the LOPC Profiles[b]

| Station | Deployment Trap Array (Start Time in UTC) | Deployment Time Trap Array (d$^{-1}$) | Gel Trap Sampling Depths (m) | Exported POC Analyzed (m) | Exported Chl *a* Analyzed (m) | Deployment Turbulence Dropsonde (Start in UTC) | Deployment LOPC (Start Time in UTC) | Number of LOPC Profiles |
|---|---|---|---|---|---|---|---|---|
| M1 | 22 Jun 2011, 15:40 | 0.22 | 30, 40, 60, 90 | 30, 40, 60 | 30, 40, 60 | 18:52 | 14:23 | 5 |
| M2 | 24 Jun 2011, 09:00 | 0.19 | 30, 40, 60, 90 | 30, 40, 60 | 30, 40, 60 | 10:44 | 18:19 | 10 |
| M4 | 27 Jun 2011, 10:40 | 0.17 | 30, 40, 60, 90 | 30, 40, 60 | | 13:37 | 13:09 | 10 |

[a]Chlorophyll *a* (Chl *a*) samples from M4 were lost.
[b]For zooplankton biomass determination.

[*Yamazaki and Osborn*, 1990], where $v$ is the temperature dependent viscosity of seawater and $\partial u'/\partial z$ is shear resolved at cm scales (with $u'$ representing horizontal velocity variation and $z$ depth)

$$S=\sqrt{\varepsilon/v} \tag{2}$$

[*Hebert and de Bruyn Kops*, 2006], and

$$K=\Gamma\varepsilon/N^2 \tag{3}$$

[*Osborn*, 1980], where $N$ is the Brunt-Väisälä buoyancy frequency and $\Gamma$ is the dissipation ratio, which is set to a typical value of 0.2 [*Moum*, 1996].

### 2.2. Suspended Biomass (Chlorophyll *a*, Dominant Phytoplankton Taxa, POC, PON)

A vertical profile of suspended biomass was collected at each sampling station at 12 depths between surface and 200 m by Niskin bottles attached to a sampling rosette (Table 1). On board the ship, the sampled water was gently transferred into carboys and stored cool and dark until filtration within few hours. Size-fractionated suspended chlorophyll *a* (Chl *a*) concentrations were determined from subsamples. Triplicates (50–200 mL) from each sampling depth were vacuum-filtered on (1) Whatman GF/F filters for the total Chl *a* ($>$0.7 $\mu$m) concentration and on (2) Whatman Nucleopore membrane filters (10 $\mu$m) for the Chl *a* size fraction $>$10 $\mu$m. Extraction of Chl *a* was subsequently conducted in 5 mL methanol for 12 h at room temperature in darkness before measuring the Chl *a* concentration using a Turner Design 10-AU fluorometer (calibrated with Chl *a*, Sigma C6144) before and after adding two drops of 5% HCl [*Holm-Hansen and Riemann*, 1978]. A 100 mL subsample of the suspended water sample was fixated with 2% glutaraldehyde lugol for phytoplankton cell counts. From the Chl *a* maximum, the most dominant species were determined by counting at least 400 cells in a 50 mL sedimentation chamber after 25 h of sedimentation [*Utermöhl*, 1931].

Triplicate subsamples (200 mL) were filtered on precombusted Whatman GF/F filters to determine the concentration of suspended particulate organic carbon (POC) and nitrogen (PON). We removed larger organisms such as copepods before freezing the filters at $-20^{\circ}$C. Within 6 months after the cruise the filters were exposed to fumes of concentrated HCl for 24 h (removal of inorganic carbon) prior to analysis on a Leeman Lab CHN Elemental Analyzer [for details see *Reigstad et al*., 2008].

### 2.3. Zooplankton Abundance

Distribution and abundance of zooplankton grazers in the water column were assessed by a laser optical plankton counter (LOPC; Rolls Royce Canada Ltd.) that was mounted on a frame together with a second CTD-F (CTD: SBE19plusV2, Seabird Inc., F: Wetlabs ECO FL fluorescence sensor). The LOPC was deployed several times at each station, and here we present data from the sampling closest in time to the deployment of the sediment traps (Table 2). At M1 and M4, the LOPC was deployed in close temporal proximity, but at M2 9 h lay between both deployments (Table 2).

During the LOPC samplings, 5–10 vertical profiles from bottom to surface were obtained at each station (Table 2). The LOPC counts particles flowing through its channel and registers their size and transparency twice per second [*Herman et al*., 2004]. Based on the LOPC data, zooplankton abundance was calculated and binned into 15 m depth intervals as described in *Gaardsted et al*. [2010] and *Basedow et al*. [2013]. To exclude transparent, carnivorous zooplankton such as hydrozoans and chaetognaths, and all possible aggregates, we limited our analyses to single element particles (SEPs) and more opaque multiple element particles (MEPs) (attenuation index $>$0.4) [see *Checkley et al*., 2008; *Basedow et al*., 2013] in the size range of 0.63–2.00 mm ESD (equivalent spherical diameter).

At the Polar Front in the Barents Sea, these plankton particles typically consist of *Calanus* spp. CI-CVI, older stages of *Pseudocalanus* spp. and some individuals of *Metridia* sp. [*Basedow et al*., 2014, and references therein].

### 2.4. Vertical Flux of Chlorophyll *a*, POC and Particles (0.050–1.139 mm)

A semi-Lagrangian drifting sediment trap array was deployed at the three sampling stations for 4–5 h (Table 2). It was anchored to a free-drifting ice floe at M1 and M2, while it was drifting in the open waters at M4. Paired sediment traps (outer diameter 72 mm, length 450 mm, KC Denmark) were arranged at sampling depths of 30, 40, 60, and 90 m to measure the vertical POC and particle flux in the vertical zone of the highest attenuation in POC export (below the euphotic zone, Table 3). Following the conceptual idea of

**Table 3.** Hydrophysical and Biological Characterization of the Sampling Stations M1, M2, and M4[a]

| Station ID | M1 | M2 | M4 |
|---|---|---|---|
| Water mass | Arctic | Polar Front | Atlantic |
| PC type | Halocline | Halocline | Thermocline |
| PC interval (m) | 7–23 | 14–21 | 35–38 |
| Density across PC (kg $m^{-3}$) | 0.96 | 1.19 | 0.15 |
| Maximal Brunt-Väisälä frequency N ($s^{-1}$) | 0.034 | 0.054 | 0.025 |
| Mixing depth (diffusivity $>10^{-4}$ $m^2$ $s^{-1}$) | 13.0 m | 17.0 m | 25.5 m |
| Euphotic zone (1% light, 430 nm) | 65 m | 54 m | 45 m |
| Nutricline ($\leq$1 $\mu$M Nitrat + Nitrit) | <20 m | <30 m | <30 m |
| Chl *a* max depth (m) | 40 | 44 | 45 |
| Chl *a* max concentration ($\mu$g $L^{-1}$) | 4.38 | 1.42 | 1.6 |
| Dominant suspended phytoplankton taxa at Chl *a* max (cells $L^{-1}$) | | | |
| *Thalassiosira* spp. | 265,000 | 3700 | |
| *Chaetoceros* spp. | 156,800 | 30,500 | 4050 |
| *Phaeocystis pouchetii* | 107,280 | 274,000[b] | 1,810,090[c] |
| Bloom stage | Late peak bloom | Late bloom | Postbloom |

[a]PC, pycnocline and Chl *a* max, chlorophyll *a* maximum.
[b]Average colony size 1.3 cells.
[c]Almost exclusively single cells.

*Lundsgaard et al.* [1999] and *Ebersbach and Trull* [2008], one of the two sediment cylinders at each sampling trap was used to determine POC and Chl *a* flux (in the following called "sediment trap"). The content of these traps was transferred into carboys right after recovery and subsampled for Chl *a* >0.7 $\mu$m, Chl *a* >10 $\mu$m, and POC. Samples were treated and analyzed as described above for the suspended water samples. The other trap cylinder at each sampling depth was equipped with a gel jar, allowing for sampling and analysis of particle size composition of sinking material (in the following called "gel trap").

Previous to deployment of the trap array in the lower euphotic zone and below it, the gel traps with Tissue-Tec® gel (Sakura Finetek Europe B.V., Netherlands) were prepared according to procedures developed by Iversen (M. H. Iversen, personal communication, 2010). Duran glass cups without spout (ø 70 mm) were filled with ca. 5 mm gel and frozen (−20°C). These cups, exactly fitting into the trap cylinder, were placed in the traps right before deployment and covered with GF/F filtered bottom water from the deployment area to allow gentle defrosting of the water soluble gel. Prefiltered (GF/F) bottom water (without fixation) was also added to the sediment traps to balance the weight of the water filled gel trap. Deployment time of 4–5 h was chosen to prevent an overload of particles in the gel traps. After recovery, the gel traps were stored dark and cold for 0.5–2 h to allow particles to sink into the gel. The overstanding water in the trap cylinder was then gently siphoned out with a silicone hose (ø 3 mm) and a 3 mL plastic pipette, but the last millimeter of water was left on the gel to prevent unintentional removal of particles. Gel jars were immediately frozen (−20°C) for later photography and image analysis ashore. Between January 2012 and June 2012, the 12 gel jars were defrosted one by one at room temperature and stored in the fridge until handling within 7 days. A preliminary test showed that storage in the fridge for a few days caused no significant decay in particle abundance and size (data not shown). The complete surface of each gel sample was photographed using a stereo microscope (15X magnification, Zeiss Discovery.V20) with an AxioCam ERc 5s digital camera (5 megapixels). Due to small changes in gel thickness and different light reflections, not all images were taken under the exact same light conditions, but a similar illumination was assured. The resulting 150–200 images (resolution 0.431 pixels/ $\mu$m) were combined into 20–25 mosaic image using the plugin MosaicJ [*Thévenaz and Unser*, 2007] in Fiji [*Schindelin et al.*, 2012]. Images were manually inspected and particles that were included in two mosaics, light reflections, bubbles in the gel, and copepods were removed. In this way, major errors were eliminated, but the amount of particles (1000–13,000 particles per glass jar) made it impossible to inspect every particle for, e.g., overlays with other particles. A minor bias must therefore be assumed. Image analysis was conducted using 8-bit gray values converted pictures. The threshold to distinguish particles from the background was determined manually for each gel jar to correct for the slight differences in the pictures' brightness. Applying the "plot profile" function of ImageJ (Figure 2), we determined an intermediate value between the maximum gray value in particles and the average of the background value by eyeballing and tested then the chosen values on several images for its ability to distinguish between particle and background noise. Threshold values for all images

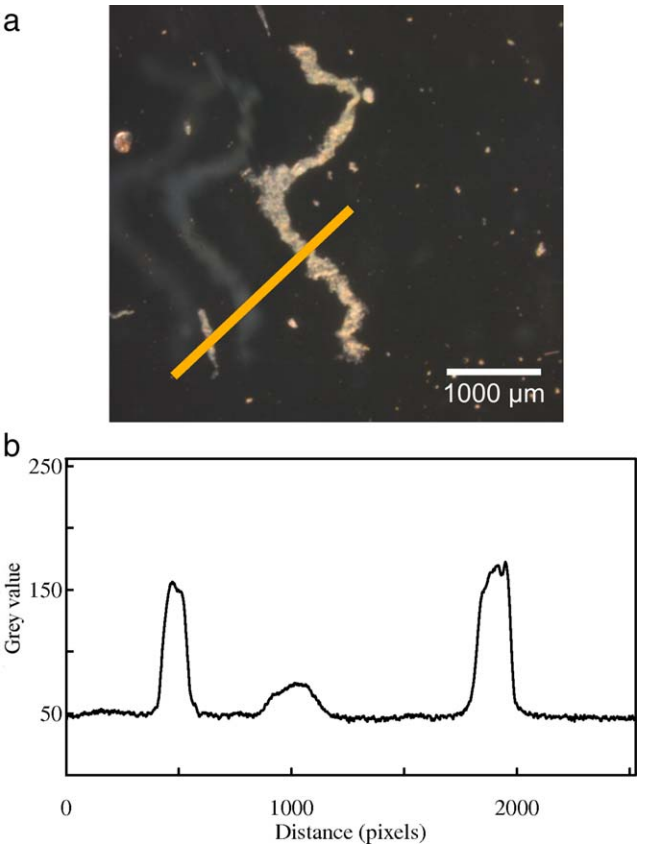


**Figure 2.** Binary pictures were produced after determining the gray value threshold between particle and background by the plot profile function of ImageJ. (a) Detail image from one gel jar with a krill fecal pellet. (b) Gray values along the yellow line (image (a)), starting at the lower left side, ending at the upper right side.

were between a gray value of 75 and 100. Based on the threshold value, the pictures were converted into binary images and the 2-D area of all particles extracted. The estimated spherical diameter was then calculated from the area of each particle. However, the ESD of particles extracted from images differs from the ESD that is estimated by the LOPC (based on light absorbance), and is more similar to the occluded diameter that can be computed for particles counted by the LOPC [*Checkley et al*., 2008]. To stress the difference between the two estimates, in the following we call the ESD estimated from images for $ESD_{image}$, in contrast to the ESD estimated by the LOPC. Since the abundance of the smallest particles in the images is underestimated due to their low spectral reflectance, the lower limit of included particles was set to 0.05 mm $ESD_{image}$ following the methods described in *Jackson et al*. [1997, 2005]. Particles within the accepted size limit were logarithmically binned according to their $ESD_{image}$ (Table 4) [following *Jackson and Checkley*, 2011]. An upper limit of the bins was chosen to be $\sqrt[3]{2} \approx 1.26$ times of the lower bin limit. We included all particles in the following analysis, since very large particles can—despite being very rare—contribute considerably to the volume flux. Particle spectra were calculated following *Jackson and Burd* [1998] to allow a comparison with other data. The volume of sinking particles was, however, computed using an ellipsoidal volume calculation, since most of the particles had this form. The third axis was here chosen to be equal with the minor axis of an ellipsis fitted to the 2-D image the fitting function of ImageJ. Volume flux was then calculated as the sum of the ellipsoidal particle volume in each bin, normalized with the sampling time, the trap cylinder opening and the bin width (to make the results comparable with other studies) and then multiplied by the bin mean (Table 4) to make the area under the curve (Figure 8) proportional to the total flux.

**Table 4.** Particle Bin Sizes Used in the Analyses and Particle Size Classification

| Bin | Bin Mean $ESD_{image}$[a] | Classification |
|---|---|---|
| 1 | 0.057 | Small Particles |
| 2 | 0.071 | |
| 3 | 0.090 | |
| 4 | 0.113 | Medium-Sized Particles |
| 5 | 0.142 | |
| 6 | 0.180 | |
| 7 | 0.226 | |
| 8 | 0.285 | |
| 9 | 0.359 | |
| 10 | 0.452 | |
| 11 | 0.570 | Large Particles |
| 12 | 0.718 | |
| 13 | 0.904 | |
| 14 | 1.139 | |
| 15 | 1.435 | Very Large (Rare) Particles |
| 16 | 1.808 | |
| 17 | 2.279 | |
| 18 | 2.870 | |

[a]ESD, equivalent spherical diameter in millimeter.

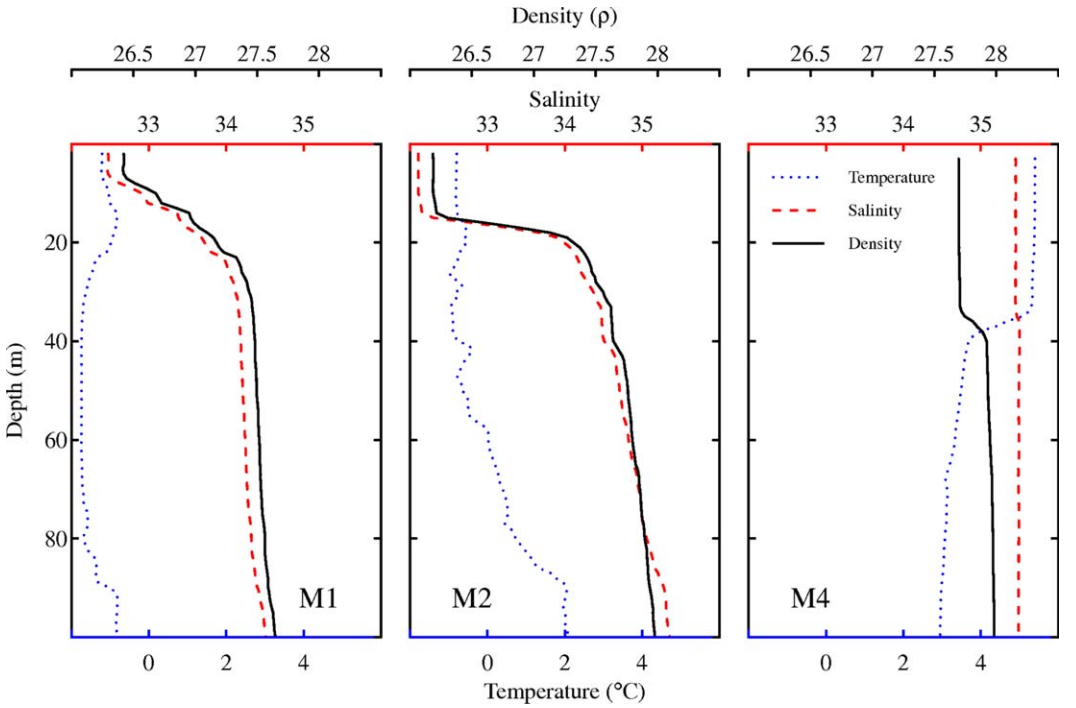


**Figure 3.** Hydrographical situation at the sampling station at (left) M1, (center) M2, and (right) M4.

Volume flux (used in the POC flux: volume flux ratio, Figure 9) was in contrast computed as the total ellipsoidal volume per bin, normalized for deployment time and sediment trap cylinder opening.

## 3. Results

### 3.1. Hydrography, Small-Scale Shear Rate, and Diffusivity Profiles

The three sampling stations in the Barents Sea (BS) differed in terms of hydrography, shear rate distribution, and vertical mixing. Very open drift ice (around 30% coverage, Table 1) was encountered at M1, the northernmost station. Water temperature was $<0^{\circ}$C throughout the upper 100 m (Figure 3), and the well-mixed surface meltwater layer (upper 5 m, salinity $\sim$32.9) was separated by a staircase-like halocline (7–23 m) from intermediate salinity water of Arctic origin (salinity 34.0–34.4 between 25 and 100 m, Figure 3). We will therefore refer to the subsurface water masses at M1 as "Arctic Water." Shear rate at 8–100 m was $<2.8\ s^{-1}$ (Figure 4a), which has been described to be the threshold fragmenting the majority of diatom aggregates [*Alldredge et al*., 1990]. Vertical diffusivity ($K$) was enhanced in the uppermost 13.0 m compared to the typical background values in deeper layers (for station intercomparison we delimited the "background diffusivity" to $<10^{-4}\ m^2\ s^{-1}$) (Figure 4b and Table 3). In the following, this zone is referred to as mixing layer, since it is actively mixed by turbulence [*Brainerd and Gregg*, 1995].

Station M2 was located in the central BS and also characterized by very open drift ice (20% coverage, Table 1). Water temperature was below 0°C in the uppermost 60 m, but increasing to 2°C at 90 m (Figure 3). A melt water layer (salinity 32.6) in the upper 15 m was separated by a strong halocline between 15 and 20 m (Table 3) from the deeper slightly warmer, intermediate saline water of Atlantic origin (salinity 35.0 at 100 m). This layering is typically observed in the Polar Front, and this station will be referred to accordingly in the following. Shear rate exceeded $2.8\ s^{-1}$ above 11 m (Figure 4a), the mixing layer depth was found in the uppermost 17.0 m characterized by a $K > 10^{-4}\ m^2\ s^{-1}$ (Figure 4b and Table 3).

At the southernmost station, M4 no seasonal sea ice was found. Water temperature was 5.4°C in the uppermost 35 m, but decreased to $\sim$3.0°C below. Salinity was very stable (35.1) down to 100 m and the station was therefore only weakly stratified, primarily by a thermocline at 35–40 m (Figure 3 and Table 3). This station was strongly influenced by Atlantic Water throughout the water column and showed a beginning summer

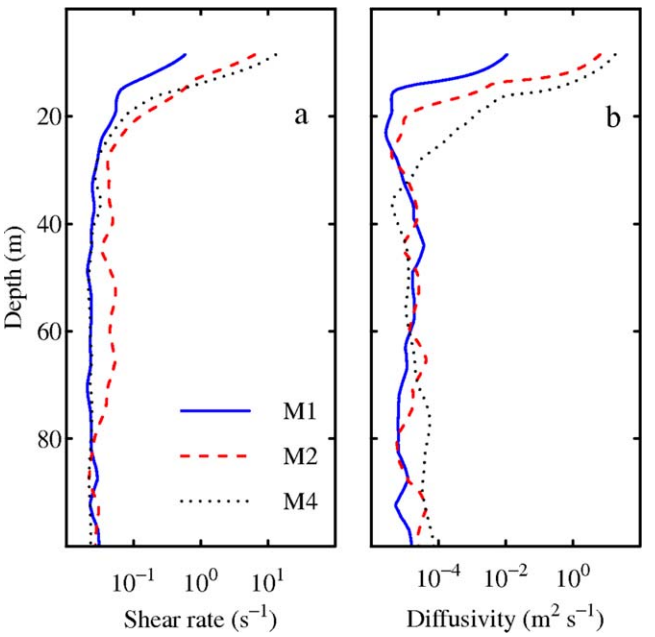


**Figure 4.** (a) Shear rate and (b) diffusivity in the upper 100 m at station M1 (blue, line), M2 (red, dashed), and M4 (black, stippled).

stratification due to warming of the upper water layers. It is therefore referred to as "Atlantic station" [*Loeng*, 1991]. Shear rate was $>2.8$ $s^{-1}$ in the 12 m top layer (Figure 4a), while the actively mixing layer with $K > 10^{-4}$ $m^2$ $s^{-1}$ reached down to 25.5 m (Figure 4b and Table 3).

### 3.2. Suspended Chlorophyll *a*, Phytoplankton Community, POC, and POC:PON Ratio

Different stages of the phytoplankton spring bloom were encountered at the three stations.

At M1 in Arctic Water, we found a distinct chlorophyll *a* maximum (Chl *a* max, 4.38 $\mu$g Chl *a* $L^{-1}$, Figure 5) at 40 m. It was dominated by large phytoplankton cells ($>10$ $\mu$m, mainly diatom genera *Thalassiosira* and *Chaetoceros*, Table 3). Single cells or small colonies (4–5 cells) of the flagellate *Phaeocystis pouchetii* ($\sim$5 $\mu$m diameter) were, however, also present (Table 3). The suspended particulate organic carbon (POC) followed the depth distribution of Chl *a* and peaked at 40 m (494 mg C $m^{-3}$, Figure 5). This suggests that the POC consisted to a great extent of autotrophic cells. The POC:PON ratio of 8.2 (atomic ratio, a:a, average of the upper 40 m) is higher than the Redfield ratio of 6.6 and points toward partly regenerated organic material above the Chl *a* max. Values of $>17$ at 90 m are too high to indicate degraded marine material [*Andreassen et al*., 1996]. Instead, resuspended or terrestrial material from ice

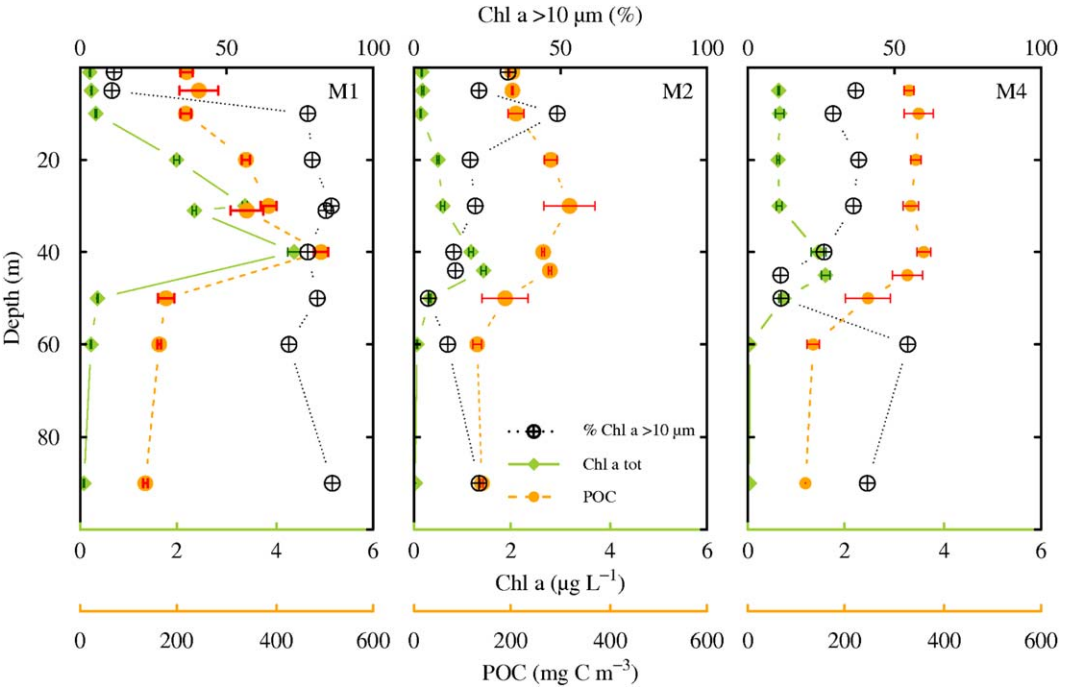


**Figure 5.** Suspended particulate organic carbon (POC, orange), suspended chlorophyll *a* (Chl *a*, green) and abundance of larger phytoplankton cells (Chl *a* $>10$ $\mu$m in % of total Chl *a*, black) in the upper 90 m at the sampling stations (left) M1, (center) M2, and (right) M4.

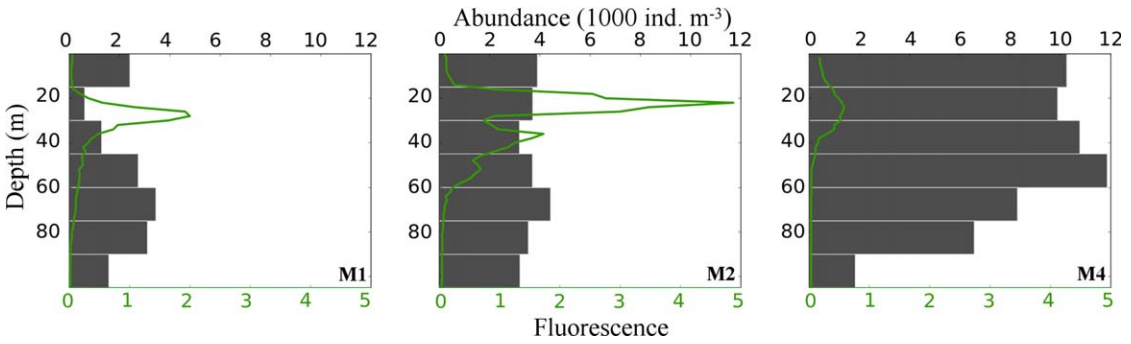


**Figure 6.** Zooplankton abundance (0.63–2.00 mm ESD, gray bars) in the upper 100 m at (left) M1, (center) M2, and (right) M4, obtained from 5 to 10 profiles of a laser optical plankton counter, and fluorescence depth profile (green line) from a CTD-F, vertically deployed together.

melting or vertical advection must be assumed. Taking into account the nutricline at <20 m (Table 3), the depth of the subsurface Chl *a* max and its concentration as well as the dominance of large diatoms, we classified this station to be in a late peak bloom stage (Table 3).

At station M2 in the Polar Front, the Chl *a* max was located slightly deeper and less distinct than at M2 (44 m: 1.42 $\mu$g $L^{-1}$, Figure 5). Single cells and few small colonies (up to eight cells) of *P. pouchetii* dominated and large cells made up only 20–50% of the autotrophic biomass. The concentration of suspended POC peaked at 30 m (318 mg C $m^{-3}$, Figure 5). A POC:PON ratio of 8.6 (a:a average of the uppermost 44 m) indicated a similar degradation of organic material down to the Chl *a* maximum at M2 compared to M1. Due to the deeper nutricline (<30 m), a subsurface Chl *a* max at 44 m with lower concentration and a higher abundance of small cells, M2 was suggested to be in a later bloom stage than M1. Since spring bloom diatoms were still present (Table 3), M2 was categorized as "late bloom", though the situation in the Polar Front was highly patchy and dynamic as indicated by variability of the Chl *a* depth distribution and the fluorescence measurements taken with the CTD-F, mounted on the same frame as the LOPC (S. Basedow, unpublished data, 2012).

The Chl *a* concentration at M4 was similar to M2, and peaked at 45 m (1.59 $\mu$g $L^{-1}$, Figure 5). The phytoplankton community however consisted almost exclusively of *P. pouchetii* single cells (Table 3). The suspended POC showed a relatively constant concentration of ~300 mg C $m^{-3}$ down to 45 m, before dropping to 120–130 mg C $m^{-3}$. An POC:PON a:a ratio of 7.7 (average down to 45 m) indicates less degraded organic material above the Chl *a* max, than at deeper layers (POC:PON >11.7 at ≥60 m) and the other sampling stations. M4 was in terms of nutricline depth (above 30 m), Chl *a* max depth, POC concentration, and POC:PON rather similar to M2, but the observed deep-mixing made a biological characterization difficult. Since, however, very few diatoms were observed, the dominant species *P. pouchetii* was accompanied by unidentified flagellates, lower fluorescence values were found, and the zooplankton community was at a later stage (C. Svensen, personal communication, 2012) compared to M1 and M2 (Figure 6), we considered M4 to be in a postbloom stage.

### 3.3. Zooplankton Abundance and Vertical Distribution

Throughout the LOPC sampling at the three stations, we observed a large temporal variability in the vertical zooplankton distribution (S. Basedow, unpublished data, 2012). Here we present data from the LOPC profiles carried out closest in time to the deployment of the sediment traps (Table 2). We limited the profiles to the upper 105 m, to convey the situation in zooplankton abundance and distribution that could have influenced the POC and particle flux into the sediment traps by grazing. Lowest abundances of zooplankton were observed at the Arctic station M1, intermediate abundances at the M2 in the Polar Front, and very high abundances of up to 12,000 individuals $m^{-3}$ at the Atlantic station M4 (Figure 6). At all stations, grazing zooplankton (0.63–2 mm ESD) was distributed relatively evenly in the upper 105 m. No relationship between the depth of the Chl *a* maximum (Figure 5) or the fluorescence maximum (Figure 6) and the vertical distribution of zooplankton could be observed.

### 3.4. Vertical Flux of Chlorophyll *a*, POC, and the POC:PON Ratio of Sinking Material

The Chl *a* and POC flux as well as the atomic (a:a) ratio POC:PON of sinking material was determined from the sediment traps. At M1, we measured a downward flux of ~3.4 mg Chl *a* $m^{-2}$ $d^{-1}$ at both 30 and 40 m, and a lower flux at 60 m (1.99 mg Chl *a* $m^{-2}$ $d^{-1}$, Table 5). Similarly to the Chl *a* flux, more POC was sinking

**Table 5.** Downward Fluxes of Chl *a* and POC[a], the POC:PON (Atomic Ratio) of the Exported Material, Average Particle Size of Sinking Particles, and Semiquantitative Abundance of the Most Abundant Particles Types Found in Gel Jars Deployed at M1, M2, and M4[b]

| | Depth (m) | Chl *a* (mg $m^{-2}$ $d^{-1}$) | POC ± SD (mg C $m^{-2}$ $d^{-1}$) | POC:PON ± SD | Average Size ($ESD_{image}$, mm) | Diatom Colonies | FP (Krill) ($10^3$ $m^{-2}$ $d^{-1}$) | FP (Copepod) | Other | Copepods |
|---|---|---|---|---|---|---|---|---|---|---|
| M1 | 30 | 3.36 | 856.2 ± 67.5 | 9.2 ± 0.4 | 0.094 | ++ | 7 | * | + | * |
| | 40 | 3.39 | 813.8 ± 29.9 | 9.5 ± 0.1 | 0.113 | ++ | 23 | + | | * |
| | 60 | 1.99 | 628.7 ± 24.9 | 9.1 ± 0.6 | 0.107 | + | **28** | + | | * |
| | 90 | | | | 0.104 | + | **17** | ++ | | |
| M2 | 30 | 0.98 | 748.6 ± 37.5 | 8.7 ± 0.4 | 0.111 | * | 9 | * | + | * |
| | 40 | 1.89 | 832.2 ± 32.5 | 9.1 ± 0.4 | 0.114 | + | **21** | + | | * |
| | 60 | 1.36 | 823.8 ± 54.7 | 9.5 ± 0.2 | 0.117 | * | **19** | + | + | + |
| | 90 | | | | 0.119 | * | **26** | + | + | * |
| M4 | 30 | | 1431.0 ± 108.7 | 7.0 ± 0.3 | 0.083 | | * | * | + | + |
| | 40 | | 1847.4 ± 169.7 | 6.2 ± 0.3 | 0.086 | * | 0 | ++ | ++ | ++ |
| | 60 | | 927.2 ± 99.6 | 7.5 ± 0.6 | 0.091 | | * | ++ | ++ | ++ |
| | 90 | | | | 0.104 | + | **36** | * | ++ | * |

[a]POC and PON concentration at 90 m are lacking.

[b]ESD, equivalent spherical diameter in millimeter; FP, fecal pellets; ++, many; +, few; *, present; dominant particle group for each depth in bold. The category "other" holds sinking particles which could not be clearly classified (detritus, different phytoplankton and zooplankton). The category "copepods" gives the number of copepods found per gel jar (maximum 60 individuals per gel jar in M4, 40 m).

out at 30 and 40 m (856.2 and 813.8 mg C $m^{-2}$ $d^{-1}$, respectively) compared to 60 m (628.7 mg C $m^{-2}$ $d^{-1}$, Table 5) at M1. The POC:PON ratio was comparable at all three depths (9.1–9.5, Table 5), indicating the outsinking of degraded marine material. At M2 less Chl *a* sank out compared to M1 (0.98–1.89 mg Chl *a* $m^{-2}$ $d^{-1}$, Table 5), though the downward POC flux with a peak at 40 m (832.2 mg C $m^{-2}$ $d^{-1}$, Table 5) was similar at both stations. Also, the POC:PON ratio was in the same range (8.7–9.5) at M1 and M2. In contrast, a much higher POC flux was observed at the deep-mixed Atlantic station M4. The POC flux for M4 at 30 and 40 m was more than twice as high as at the other stations (1431 and 1847 mg C $m^{-2}$ $d^{-1}$, Table 5). The flux at 60 m was, however, <30% greater at M4 than at M1 and M2. The POC:PON ratio of 6.2–7.5 was consistent with the Redfield ratio of 6.6, suggesting a downward flux of relatively fresh and high quality organic material relative to the more northern stations.

### 3.5. Numbers and Size-Spectra of Exported Particles

A qualitative assessment of the gel jars indicates that composition of sinking particles differed at M1, M2, and M4 (exemplified by mosaic images from 60 m, Figure 7). Based on the image analyses, we conclude small particles were most important for the vertical flux at the Atlantic station (average over all depths 0.091 mm $ESD_{image}$, Table 5). At M2 in the Polar Front the size of sinking particles was on average largest (ESD 0.115 mm, Table 5). At both stations, the size increased with depth. Particles from the Arctic station were of intermediate size (ESD 0.104 mm, Table 5), and though they became larger between 30 and 40 m, size decreased down to 90 m. Adding all depth, the number of exported particles was lowest at M2 ($167 \times 10^6$ particles), intermediate at M4 ($450 \times 10^6$ particles), and highest at M1 ($533 \times 10^6$ particles). Also, small particles (0.05–0.1 mm $ESD_{image}$, Table 4) were at all sampling depths more abundant than large ones (0.50–1.14 mm $ESD_{image}$, Figure 8).

The highest number of particles per sampling depth was found in the gel jar deployed at 40 m at station M4 ($2.61 \times 10^6$ particles $m^{-2}$ $d^{-1}$). Small and medium-sized particles were more abundant at 40 m than 30 m at this station, but their numbers decreased again at 60 m. Large and extralarge particles were rare (1–4 particles per gel jar) at these three depths, but large particles were more frequently observed at 90 m (Figure 8e). In the gel jar deployed at 30 m at M1, we found the second highest number of particles ($2.25 \times 10^6$ particles $m^{-2}$ $d^{-1}$). At this station, small and medium-sized particles (0.05–0.50 mm $ESD_{image}$, Table 4) became less abundant with depth (Figure 8a), while large particles (0.50–1.14 mm $ESD_{image}$, Table 4) were most abundant at 40 and 60 m (Figure 8a). At M2, we found fewest particles at 30 m while most were observed at 40 m (Figure 8c).

The volume of exported particles is reflected by the area under the curve in the volume flux spectra (Figures 8b, 8d, and 8f). All spectra demonstrate that small particles contributed little to the volume export at the three sampling stations, despite their high abundance. In contrast, large and extralarge particles explained most of the downward volume flux. The highest volume fluxes were found at 40 m at M1 and M2 (Figures 8b and 8d). Due to the low magnification (15X) in the image analysis, only a semiquantitative particle identification was achievable, but a higher magnification would have enhanced the problem of choosing the level of

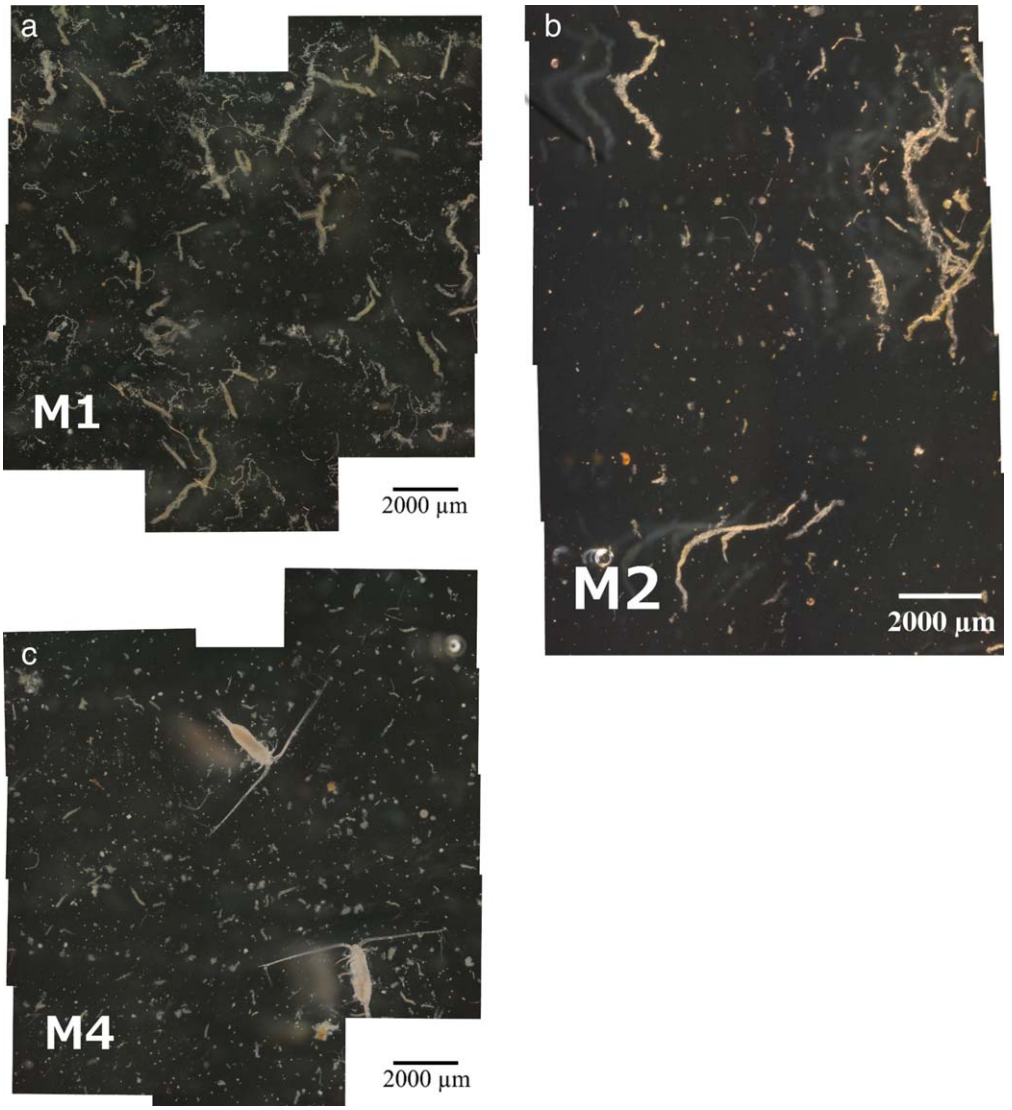


**Figure 7.** Qualitative support for the observations at station (a) M1, (b) M2, and (c) M4. Note that copepods and nauplii (in M4) were removed before the image analysis was conducted.

focus in the gel. Accordingly, we can state that mainly diatom colonies were exported at 30 and 40 m at station M1, while krill and copepod fecal pellets dominated at 60 and 90 m (Table 5). Krill pellets fragments were enumerated (23–93 per gel jar, corresponding with up to 7–27 $\times$ $10^3$ pellet fragments $m^{-2}$ $d^{-1}$, Table 5). Since krill pellets are filiform, without defined tips and easily break apart [*Wexels Riser et al*., 2007], the fragments vary in size. They can therefore not be used as defined fecal pellet units corresponding to a defined volume flux.

The low particle abundance at 30 m at M2 resulted also in a low volume flux. It was difficult to identify the small and medium-sized particles exported here, consisting mainly of fecal pellets and fine detritus (Table 5). At the other sampling depths at M2 large krill fecal pellets and diatom colonies dominated.

Gel jars deployed at M4 (30, 40, and 60 m) contained mainly small unidentifiable particles, assumingly detritus, as well as several benthic larvae. In addition, we found a remarkably high number of copepods (up to 60 individuals) in the 40 and 60 m gel jar (Table 5). Since only 1–2 individuals were found per glass jar at most other sampling depths, and individuals fallen into the gel were not able to continue grazing due to the high gel viscosity, we do not regard the short-term sediment traps with gel jar we used as generally more attractive to copepods. Small unidentified particles and krill fecal pellets dominated in the 90 m jar at M4 (36 $\times$ $10^3$ pellets $m^{-2}$ $d^{-1}$, Table 5).

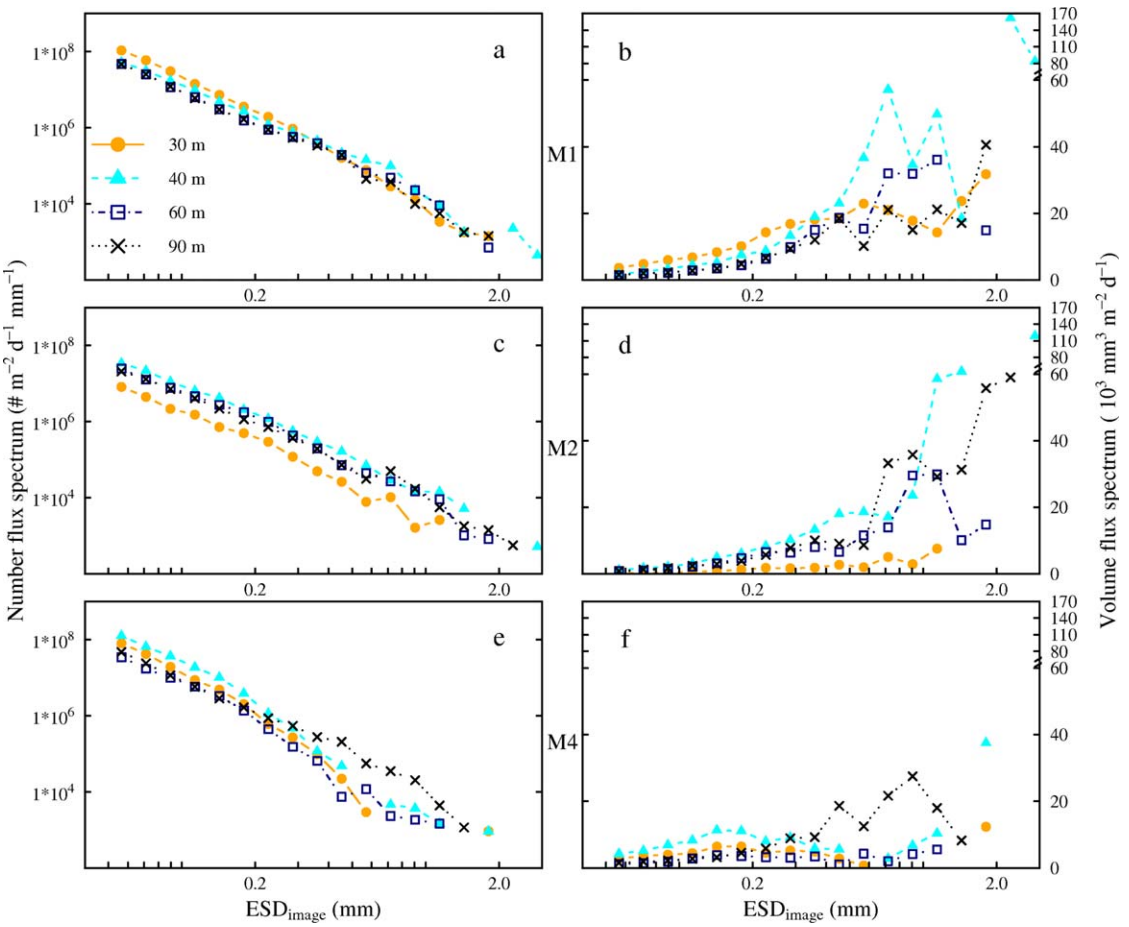


**Figure 8.** (Left) Number size spectra and (right) computed volume flux spectrum of particles collected in the gel traps at 30, 40, 60, and 90 m (top: M1, middle: M2, bottom: M4). Note that the broken *y* axis in the right column.

## 4. Discussion

In the present study, we investigated the vertical fluxes and characteristics of sinking particles in the central Barents Sea (BS) along a north-south transect from Arctic Water, crossing the Polar Front, to Atlantic Water. Along this track, we expected to meet contrasting situations with respect to hydrography, small-scale turbulence, vertical mixing, phytoplankton spring bloom stage, zooplankton abundance, and vertical export rates of particulate organic carbon (POC). We anticipated that there would be a (late) peak spring bloom and a high POC flux at station M1 in the stratified Arctic Water, an "intermediate stage" spring bloom and POC flux at M2 in the Polar Front, and strong POC retention in the Atlantic deep-mixed, postbloom waters at M4. Surprisingly, the POC export at 60 m was ~30% higher at M4 in Atlantic Water compared to the flux at station M1 in Arctic Water (930 versus 630 mg C $m^{-2}$ $d^{-1}$) even if large and extralarge sinking particles (0.5–2.8 mm equivalent spherical diameter, $ESD_{image}$, Table 4) were extremely rare down to 60 m at M4.

To explore the impact of physical and biological processes on the size spectra of sinking particles and the POC flux, we evaluate the role of small-scale turbulence, phytoplankton and zooplankton abundance on the particle size spectra and then discuss if a high POC flux is always associated with large sinking particles (>0.5 mm $ESD_{image}$) like diatom aggregates, marine snow, and krill fecal pellets.

### 4.1. Influence of Small-Scale Shear Rate and Diffusivity on the Particle Size Spectra and the POC Flux

Small-scale shear rates in the range of 0.02–13.11 $s^{-1}$ were calculated for the upper 100 m at the three sampling stations (Figure 4a) and the maximum rates computed in our study somewhat exceeded previously reported shear rates for the inner ocean and estuaries ($10^{-7}$–10 $s^{-1}$) [*Kiørboe et al.*, 1990, and citations therein].

An enhanced shear rate is commonly assumed to facilitate the coagulation of particles into larger, usually faster sinking aggregates by increasing the collision rate of suspended particles [*McCave*, 1984; *Jackson*, 1990].

However, the shear rate in the uppermost 11–12 m of station M2 and M4 was $>2.8\ s^{-1}$ (corresponding to an energy dissipation rate $>0.001\ m^2\ s^{-3}$) exceeded a threshold, which has been suggested to fragment the majority of diatom aggregates [*Alldredge et al*., 1990]. This indicates that particle aggregation was not promoted in the surface layer at M2 and M4. At the deeper chlorophyll *a* maximum (Chl *a* max) depths, the shear rates were however $\leq 0.035\ s^{-1}$ at all three sampling stations, resulting in a theoretical particle maximum size of $\leq 5$ mm $ESD_{image}$ [*Jackson*, 1990]. Particles in all deployed gel traps had $ESD_{image}$ <3.2 mm, and were well below this upper theoretical size limit.

We conclude that shear rates at station M1 at all depths were in a range facilitating formation of larger particles. Diatoms, which are known to excrete a natural "glue" for particle formation [*Alldredge*, 2001], were also abundant here (Table 3) and may have promoted particle aggregation further. In contrast, the formation of larger particles may have been limited by the high shear rate in the uppermost 10 m at M2 and M4. This is however not assumed to have a strong effect on particle aggregation, since the Chl *a* max, the zone of highest biomass, particle abundance and accordingly particle aggregation, was located well below this layer of high shear rate (Figure 4a and Table 3).

The vertical diffusivity (*K*) indicates a mixing layer of 13.0, 17.0 m, and 25.5 m at M1, M2, and M4, respectively. This means that enhanced, surface-driven vertical mixing reached considerably deeper (>10 m) at the sampling station in Atlantic Water compared to the stations in Arctic Water or the Polar Front. A deeper mixing at M4 may enhance the sinking speed, with consequently reduced exposure time for degradation processes to take place [*Svensen et al*., 2012], and can help explain the high POC flux and the presence of rather fresh material down to 60 m at this station (Table 5, POC:PON ratio of exported material of 6.2–7.5 compared to the Redfield ratio of 6.6).

### 4.2. Flux of Autotrophic Biomass in Form of Small and Large Particles

The concentrations of suspended Chl *a* at the deep chlorophyll maximum were highest in the late peak bloom situation at M1 and lowest during the late bloom station at M2 (Figure 5 and Table 3). This may contradict our bloom classification into M1 "late peak bloom," M2 "late bloom," M4 "postbloom" at the first sight, but frequent LOPC deployments at M2 indicated a high short-time variability in the relative pigment distribution fluorescence measurements especially in the Polar Front. During six deployments at station M2 (within 30 h), the fluorescence peak changed from >500 to <100 (relative units) (S. Basedow, unpublished data, 2012). A direct comparison between Niskin-bottle based Chl *a* concentrations and the closest in time fluorescence from LOPC profiling was therefore not feasible (Figures 5 and 6, linear regression, $R^2 = 0.2–0.3$). Instead, this reflects the previously reported strong spatial variability in the Polar Front [*Våge*, 2010], and indicates the importance of including not only Chl *a* concentrations, but also hydrography, euphotic depth, nutricline, and the zooplankton composition in the bloom stage characterization as it was done in the present study.

At the Arctic Water station M1, we found a high number of particles <0.05 mm $ESD_{image}$ in the 30 m gel trap. These particles were not included in the image analysis due to underestimation concerns for particles this small (see section 2) and we could not identify them visually in the jars. The high Chl *a* export at this sampling depth at M1 (Table 5) however suggests the export of autotrophs. *Thalassiosira* single cells (10–50 $\mu$m diameter) [*Hasle and Syvertsen*, 1997] or short chains were highly abundant in the sediment traps deployed for 24 h during the present cruise (M. Reigstad et al., unpublished data, 2012) and it is likely that this genus was also abundant in the gel jars. Diatoms and their resting spores have previously been described to sink with velocities of $>10\ m\ d^{-1}$ [*Smayda*, 1970] and they represented one of the most abundant particle groups in gel traps deployed along the Antarctic Peninsula [*McDonnell and Buesseler*, 2010]. Despite the unquestionable importance of large particles in the downward mass transport, we argue accordingly that it is important to keep in mind that also particles <0.05 mm $ESD_{image}$ do sink and can contribute to the vertical export, especially if their density is high enough or if the particles are ballasted [*Iversen et al*., 2010].

In terms of mass flux, sinking diatom aggregates are much more important than single cells. They form an important vehicle of POC export and they were highly abundant in the gel jar deployed at 40 m at M1 (Table 5). The genera *Chaetoceros* and *Thalassiosira* dominated the suspended phytoplankton sample taken at this station (Table 3) and were also found in the 24 h deployed sediment traps (M. Reigstad et al., unpublished data, 2012). We suggest accordingly that they contributed to aggregate formation at M1, especially since some species in these genera are known to have potentially sticky cells or produce adhesive extracellular substances [*Kiørboe*

*and Hansen*, 1993; *Hansen and Kiørboe*, 1997], the natural "glue" in aggregate formation [*Alldredge*, 2001]. However, even if the particle spectra from M1 indicate a shift from many small particles at 30 m (0.05–0.1 mm $ESD_{image}$) to a majority of particles >0.9 mm $ESD_{image}$ at 40 m, our data cannot confirm that this was solely due to aggregate formation. Also cell growth and increasing length of chains may have contributed to enhanced particle size.

*Phaeocystis pouchetii* single cells (5 $\mu$m) and small colonies clearly dominated the Chl *a* max at station M4 (45 m: $>1.8 \times 10^6$ suspended cells $L^{-1}$). This cell number exceeded the total phytoplankton cell abundance at the other stations by more than one order of magnitude. Based on the high cell number, a substantial cell collision rate and a potentially high aggregate formation may have been anticipated. Conversely, *P. pouchetii* has been shown to have low stickiness [*Passow and Wassmann*, 1994] and cell counts from the sediment traps deployed for 24 h during the present cruise (M. Reigstad et al., unpublished data, 2012), indicate that mainly single cells or small colonies were sinking out at 60 m. This may contradict previous results that cells <5 $\mu$m ESD are too small to sink [*Legendre and Rivkin*, 2002]. However, at M4, we also observed vertical mixing down to 35–38 m (Table 3), and assumed that this mixing enhanced the vertical transport of *P. pouchetii* cells down to the mixed depth. As phytoplankton grows mainly in the illuminated upper water layers, deep mixing can contribute to the distribution of biomass also deeper layers (with initially lower cell concentrations) and may then result in a greater contribution of phytoplankton cells to the higher carbon flux. *Olli et al.* [2002] and *Reigstad and Wassmann* [2007] described this previously, when *P. pouchetii* single cells were exported in substantial amounts (60–200 mg C $m^{-2}$ $d^{-1}$) to >90 m.

### 4.3. Potential Impact of Zooplankton on the Particle Size Spectrum

Zooplankton can influence the size spectrum of sinking particles and the vertical POC flux in various ways: They can (1) generally reduce the number of particles due to grazing, (2) contribute to the formation of larger particles (fecal pellets) by repackaging small food particles into fecal pellets, and (3) modify the particle size spectra toward smaller particles due to fragmentation of both fecal pellets and aggregates [*Wexels Riser et al.*, 2007]. Data from the LOPC indicate that abundances of grazers in the size range of 0.63–2.00 mm ESD (different stages of *Calanus* spp.) reached up to 12,000 individuals $m^{-3}$ at M4 in Atlantic Water (Figure 6). We can therefore assume that the effect of zooplankton was strongest at M4.

The combined approach of particle size spectra (Figure 8) and the semiquantitative analysis of the material in the gel jars (Table 5) also showed that copepod fecal pellets (FP) were frequently sinking out at 40 and 60 m at M4 (Table 5 and Figure 8f: particles 0.10–0.35 mm $ESD_{image}$ in the volume flux spectra match *Calanus* spp. FP sizes [*Wexels Riser et al.*, 2002]). This indicates that the comparable low Chl *a* concentrations at M4 with a prevailing phytoplankton community of <10 $\mu$m (Figure 5) could sustain a considerable zooplankton population with a high FP production that provided an important vehicle for vertical carbon flux in this postbloom situation. The great amount of unidentifiable detritus at M4 may also origin from FP, but being modified to smaller particles through fragmentation. The copepod species, *Calanus finmarchicus*, abundant at M4 (C. Svensen, personal communication, 2012) has been shown to impact the particle size spectra through unintended fragmentation of FP while feeding [*Svensen et al.*, 2012].

In addition, krill pellets fragments were abundant at most sampling depths at M1 and M2, as well as 90 m at M4 (Table 5), matching previous findings from the region [*Wexels Riser et al.*, 2002] and confirming, that krill pellets form, besides diatom aggregates and copepod pellets, an important pathway of downward carbon flux. Since krill pellets however easily break apart when being produced, the number of pellets and pellet fragments does not give a good approximation to the actual biomass sinking out.

Grazing has been described to take place associated with thin layers of enhanced particle abundance [*Möller et al.*, 2012], often formed at strong density gradients [*Alldredge et al.*, 2002; *Prairie et al.*, 2013]. Prior to the sampling, we therefore assumed that a strong vertical gradient in particle size spectra resulting from thin layer distribution of grazers, modifying the particle composition, would be detected by the high vertical resolution of sediment traps. Our LOPC data did however indicate a rather even zooplankton distribution in the upper 90 m at all three stations, neither associated with a density gradient or layers of high autotrophic biomass, which could serve as preferred feeding sites (Figure 6). Neither did we see a strong vertical shift in particle size spectra. Furthermore, no evidence for a synchronized diurnal vertical migration (DVM) could be identified during the sampling period (S. Basedow, unpublished data, 2012), supporting previous observations from the Arctic summer with 24 h of day light [*Blachowiak-Samolyk et al.*, 2006; *Wexels Riser et al.*, 2007]. The particle modification by zooplankton therefore seemed to take place over a wide vertical zone, and this distribution could be

expected to increase the attenuation and reduce vertical flux. Still, the POC flux was high at 60 m on the M4 station.

### 4.4. Linking the Downward Flux of POC and Particles >0.05 mm $ESD_{image}$

The POC fluxes measured during the present study (30–90 m: 630–1850 mg C $m^{-2}$ $d^{-1}$) match previously reported values from the upper 200 m of the central BS during spring (<2000 mg C $m^{-2}$ $d^{-1}$) [*Olli et al*., 2002; *Reigstad et al*., 2008]. It was however unexpected that the POC flux in the 4–5 h deployed traps of the present study (60 m: 628–927 mg C $m^{-2}$ $d^{-1}$) exceeded the export measured in the subsequently deployed 24 h sediment traps (60 m: 208–322 mg C $m^{-2}$ $d^{-1}$) (M. Reigstad et al., unpublished data, 2012). *Lampitt et al*. [1993] reported a strong diurnal variability in the marine snow abundance, and suggested variation in the diel production and export to cause it. An analogous reason may have contributed to the variability in the POC flux in our results. Despite no DVM was observed, there may be diurnal variability in feeding activity influencing the flux. *Juul-Pedersen et al*. [2006] stated that a deployment time of 6 or 24 h did not change the results of the measured carbon flux significantly in a Greenlandic fjord. Since the 24 h deployments of the traps used in the present study have previously been calibrated through comparison with thorium-based flux measurements in the Barents Sea and found good [*Coppola et al*., 2002], we suggest further investigation of the potential diurnal flux variability.

The deployment of the gel jars revealed that a high particle number flux (up to $10^9$ particles $m^{-2}$ $d^{-1}$ $mm^{-1}$) takes place in the Arctic, Polar Front, and Atlantic part of the BS. These fluxes exceed the number of particles found in studies conducted in the Southern Ocean by up to 3 orders of magnitude [*Ebersbach and Trull*, 2008; *McDonnell and Buesseler*, 2010; *Ebersbach et al*., 2011]. In addition particles <0.05 mm $ESD_{image}$ were highly abundant in our gel traps deployed in the BS, while *Ebersbach and Trull* [2008] excluded particles <0.15 mm ESD since they were infrequently observed. These results may hint toward major differences in particle flux in the two ecosystems [present study: uppermost 90 m on productive Arctic shelf, *Ebersbach and Trull*, 2008; *Ebersbach et al*., 2011: 100–439 m in the open Southern Ocean off Kerguelen Island and Tasmania], the sampling period [present study: early European summer, *Ebersbach and Trull*, 2008; *Ebersbach et al*., 2011: late Austral summer] methodological differences like gel type [present study: Tissue tec gel®, *Ebersbach and Trull*, 2008; *Ebersbach et al*., 2011: acrylamide], trap aspect ratio [present study: 6.4, *Ebersbach and Trull*, 2008; *Ebersbach et al*., 2011: 5], or a combination of different factors.

Previous to our study, we anticipated a higher POC export at the late peak bloom station M1 in Arctic Water compared to the late bloom at M2 in the Polar Front and the postbloom at M4 in Atlantic Water. A high suspended biomass of diatoms during the (late) peak bloom (M1) was expected to result in an enhanced export of large aggregates, while the postbloom scenario (M4) was supposed to have a high carbon turn over and a prevailing POC retention [*Wassmann*, 1998]. However, our results indicate a higher POC flux in the well-mixed Atlantic part compared to the Arctic part or the Polar Front. High flux combined with weak stratification has previously been described from this area during spring and summer [*Olli et al*., 2002; *Reigstad et al*., 2008]. It was surprising to find this high POC export combined with the, on average, smallest particles at M4 (Table 5). Large and extralarge particles were here very rare compared to M1 and M2. However, when a POC: volume ratio is calculated from all sampling depths (Figure 9), it becomes obvious, that sinking particles at M4 had a higher POC: volume content than particles at M1 and at most depths at M2. The ratios calculated for M4 are

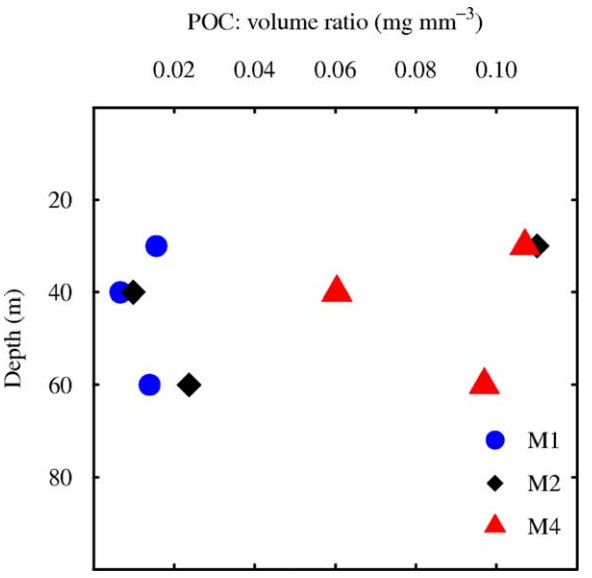


**Figure 9.** Average POC:volume ratio of the particles found in the gel traps. Note: No POC samples were available for 90 m and sample M2, 30 m contained very few particles, which makes the result probably biased.

**Table 6.** Literature Values on the Carbon Conversion Factor (mg C $mm^{-3}$) of Diatom Aggregates and Different Fecal Pellet Types

| Reference | Carbon Conversion Factor (mg C $mm^{-3}$) | Particle Type |
|---|---|---|
| *Alldredge* [1998] | 0.0001–0.003 | Diatom aggregates |
| *Wexels Riser et al.* [2007] | 0.045 | Euphausiid fecal pellets |
| *Riebesell et al.* [1995] | 0.0694 | Copepod fecal pellets |
| *Reigstad et al.* [2005] | 0.0803 | *Calanus finmarchicus* fecal pellet |
| *Wexels Riser et al.* [2007] | 0.0943 | *Calanus glacialis* fecal pellet |

comparable with fecal pellet carbon: volume ratios, and suggest the downward flux was of copepod fecal pellet origin (Table 6). Those from M1 and 40 and 60 m samples from M2 correspond in contrast to the carbon:volume ratios described for diatom aggregates [*Alldredge*, 1998].

Since these signals are also in agreement with the semiquantitative observations from the gel jars, we suggest that the high abundance of copepods and their repackaging of material into fecal pellets played a major role in enhancing the flux at station M4 compared to M1 and M2, despite that the fecal material was partly fragmented, probably resulting in reduced sinking rates.

## 5. Conclusion

Enhanced POC export is often linked to a late (peak) bloom situation and strong downward flux of large, fast-sinking particles like phytoplankton aggregates, marine snow, and zooplankton fecal pellets [*Riebesell*, 1991; *Alldredge*, 2001]. The results from the sediment traps (partly modified with gel jars) deployed in the Arctic influenced part of the Barents Sea (BS) confirm this (POC, 60 m: 629 mg C $m^{-2}$ $d^{-1}$). However, our study also indicate that an even higher vertical POC export (60 m: 927 mg C $m^{-2}$ $d^{-1}$) took place in at the deep-mixed, postbloom sampling station in the Atlantic influenced part of the BS. Here many small and medium-sized particles (0.05–0.5 mm $ESD_{image}$) were observed down to 60 m, while larger ones were rare. Coagulation into larger particles appeared to play a minor role in this case, due to the low stickiness of the most abundant phytoplankton taxon *Phaeocystis pouchetii*, but the producing fast-sinking fecal pellets obviously enhanced the vertical transport substantially, despite a high degree of fragmentation, resulting in a small average particle size.

We argue accordingly that the general concept of associating large, fast-sinking particles of phytoplankton origin with an export dominated system during the late peak bloom or late bloom phase contrasting small, slow-sinking particles with a postbloom retention dominated system, is not valid at all instances: we observed that an enhanced POC export can not only take place in form of diatom aggregates during the late bloom, but also in a deeper mixed, postbloom situation dominated by *Phaeocystis pouchetii*. This scenario co-occurred with a substantial zooplankton community. The flux was mainly characterized by small and medium-sized particles (0.05–0.5 mm $ESD_{image}$), and the POC:volume ratio matched fecal pellets. Zooplankton modification is therefore a likely driver of this high flux.

By including not only the POC flux, but also the size of sinking particles, the obtained, highly variable POC:-volume ratio may help identifying the source and mechanisms driving the downward flux of organic material. Understanding the mechanisms and attenuation of flux better, and including this into ecosystem- and carbon flux models, will improve predictions of future vertical carbon flux resulting from changing climate and the resulting pelagic ecosystem, where both the phytoplankton and zooplankton communities may change.

**Acknowledgments**
The authors would like to thank the captain and the crew of the R/V "Helmer Hanssen" for practical assistance during the fieldwork and C. Svensen, C. Wexels Riser, and S. Øygaarden for a helping hand during the filtration aboard and the CHN analysis. The detailed comments of two anonymous reviewers were highly appreciated and improved the paper substantially. The conducted work was part of the CONFLUX project, funded by Tromsø Forskningsstiftelse and Sundfjord's participation was also funded by the Centre for Ice, Climate, and Ecosystems (ICE) at the Norwegian Polar Institute.

## References

Alldredge, A. (1998), The carbon, nitrogen and mass content of marine snow as a function of aggregate size, *Deep Sea Res., Part I*, *45*(4–5), 529–541, doi:10.1016/S0967-0637(97)00048-4.

Alldredge, A. (2001), Particle aggregation dynamics, in *Encyclopedia of Ocean Sciences*, edited by J. H. Steele, S. A. Thorpe, and K. K. Turekian, pp. 2090–2097, Academic, San Diego, Calif., doi:10.1006/rwos.2001.0468.

Alldredge, A. L., T. C. Granata, T. D. Gotschalk, and T. D. Dickey (1990), The physical strength of marine snow and its implications for particle disaggregation in the ocean, *Limnol. Oceanogr.*, *35*(7), 1415–1428, doi:10.4319/lo.1990.35.7.1415.

Alldredge, A. L., T. J. Cowles, S. MacIntyre, J. E. B. Rines, P. L. Donaghey, Ch. F. Greenlaw, D. V. Holliday, M. M. Dekshenieks, J. M. Sullivan, and J. R. V. Zaneveld (2002), Occurrence and mechanisms of formation of a dramatic thin layer of marine snow in a shallow Pacific fjord, *Mar. Ecol. Prog. Ser.*, *233*, 1–12, doi:10.3354/meps233001.

Andreassen, I., E. Nöthig, and P. Wassmann (1996), Vertical particle flux on the shelf off northern Spitsbergen, Norway, *Mar. Ecol. Prog. Ser.*, *137*, 215–228, doi:10.3354/meps137215.

Basedow, S. L., K. S. Tande, M. F. Norrbin, and S. A. Kristiansen (2013), Capturing quantitative zooplankton information in the sea: Performance test of laser optical plankton counter and video plankton recorder in a *Calanus finmarchicus* dominated summer situation, *Prog. Oceanogr.*, *108*, 72–80, doi:10.1016/j.pocean.2012.10.005.

Basedow, S. L., M. Zhou, and K. S. Tande (2014), Secondary production at the Polar Front, Barents Sea, August 2007, *J. Mar. Syst.*, *130*, 147–159, doi:10.1016/j.jmarsys.2013.07.015.

Blachowiak-Samolyk, K., S. Kwasniewski, K. Richardson, K. Dmoch, E. Hansen, H. Hop, S. Falk-Petersen, and L. T. Mouritsen (2006), Arctic zooplankton do not perform diel vertical migration (DVM) during periods of midnight sun, *Mar. Ecol. Prog. Ser.*, *308*, 101–116, doi:10.3354/meps308101.

Brainerd, K. E., and M. C. Gregg (1995), Surface mixed and mixing layer depths, *Deep Sea Res., Part I*, *42*(9), 1521–1543, doi:10.1016/0967-0637(95)00068-H.

Checkley, D. M., Jr., R. E. Davis, A. W. Herman, G. A. Jackson, B. Beanlands, and L. A. Regier (2008), Assessing plankton and other particles in situ with the SOLOPC, *Limnol. Oceanogr.*, *53*(5, part 2), 2123–2136, doi:10.4319/lo.2008.53.5_part_2.2123.

Coppola, L., M. Roy-Barman, P. Wassmann, S. Mulsow, and C. Jeandel (2002), Calibration of sediment traps and particulate organic carbon export using 234Th in the Barents Sea, *Mar. Chem.*, *80*(1), 11–26, doi:10.1016/S0304-4203(02)00071-3.

Ebersbach, F., and T. W. Trull (2008), Sinking particle properties from polyacrylamide gels during the Kerguelen Ocean and Plateau compared Study (KEOPS): Zooplankton control of carbon export in an area of persistent natural iron inputs in the Southern Ocean, *Limnol. Oceanogr.*, *53*(1), 212–224, doi:10.2307/40006162.

Ebersbach, F., T. W. Trull, D. M. Davies, and S. G. Bray (2011), Controls on mesopelagic particle fluxes in the Sub-Antarctic and Polar Frontal Zones in the Southern Ocean south of Australia in summer—Perspectives from free-drifting sediment traps, *Deep Sea Res., Part II*, *58*(21–22), 2260–2276, doi:10.1016/j.dsr2.2011.05.025.

Gaardsted, F., K. S. Tande, and S. L. Basedow (2010), Measuring copepod abundance in deep-water winter habitats in the NE Norwegian Sea: Intercomparison of results from laser optical plankton counter and multinet, *Fish. Oceanogr.*, *19*(6), 480–492, doi:10.1111/j.1365-2419.2010.00558.x.

Gifford, D. J., L. M. Fessenden, P. R. Garrahan, and E. Martin (1995), Grazing by microzooplankton and mesozooplankton in the high-latitude North Atlantic Ocean: Spring versus summer dynamics, *J. Geophys. Res.*, *100*(C4), 6665–6675, doi:10.1029/94JC00983.

Hamm, C., M. Reigstad, C. W. Riser, A. Mühlebach, and P. Wassmann (2001), On the trophic fate of *Phaeocystis pouchetii*. VII. Sterols and fatty acids reveal sedimentation of *P. pouchetii*-derived organic matter via krill fecal strings, *Mar. Ecol. Prog. Ser.*, *209*, 55–69, doi:10.3354/meps209055.

Hansen, J. L. S., and T. Kiørboe (1997), Quantifying interspecific coagulation efficiency of phytoplankton, *Mar. Ecol. Prog. Ser.*, *159*, 75–79, doi:10.3354/meps159075.

Hasle, G. R., and E. E. Syvertsen (1997), Marine diatoms, in *Identifying Marine Phytoplankton*, edited by C. R. Tomas, pp. 5–385, Academic, San Diego, Calif.

Hebert, D. A., and S. M. de Bruyn Kops (2006), Relationship between vertical shear rate and kinetic energy dissipation rate in stably stratified flows, *Geophys. Res. Lett.*, *33*, L06602, doi:10.1029/2005GL025071.

Herman, A. W., B. Beanlands, and E. F. Phillips (2004), The next generation of optical Plankton counter: The laser-OPC, *J. Plankton Res.*, *26*(10), 1135–1145, doi:10.1093/plankt/fbh095.

Hodal, H., and S. Kristiansen (2008), The importance of small-celled phytoplankton in spring blooms at the marginal ice zone in the northern Barents Sea, *Deep Sea Res., Part II*, *55*(20–21), 2176–2185, doi:10.1016/j.dsr2.2008.05.012.

Holm-Hansen, O., and B. Riemann (1978), Chlorophyll *a* determination: Improvements in methodology, *Oikos*, *30*(3), 438–447, doi:10.2307/3543338.

Ingvaldsen, R., and H. Loeng (2009), Chapter 2: Physical oceanography, in *Ecosystem Barents Sea*, edited by E. Sakshaug, G. H. Johnsen and K. M. Kovacs, pp. 33–64, Tapir, Trondheim, Norway.

Iversen, M. H., N. Nowald, H. Ploug, G. A. Jackson, and G. Fischer (2010), High resolution profiles of vertical particulate organic matter export off Cape Blanc, Mauritania: Degradation processes and ballasting effects, *Deep Sea Res., Part I*, *57*(6), 771–784, doi:10.1016/j.dsr.2010.03.007.

Jackson, G. A. (1990), A model of the formation of marine algal flocs by physical coagulation processes, *Deep Sea Res., Part A*, *37*(8), 1197–1211, doi:10.1016/0198-0149(90)90038-W.

Jackson, G. A., and A. B. Burd (1998), Aggregation in the marine environment, *Environ. Sci. Technol.*, *32*(19), 2805–2814, doi:10.1021/es980251w.

Jackson, G. A., and D. M. Checkley (2011), Particle size distributions in the upper 100 m water column and their implications for animal feeding in the plankton, *Deep Sea Res., Part I*, *58*(3), 283–297, doi:10.1016/j.dsr.2010.12.008.

Jackson, G. A., R. Maffione, D. K. Costello, A. L. Alldredge, B. E. Logan, and H. G. Dam (1997), Particle size spectra between 1 $\mu$m and 1 cm at Monterey Bay determined using multiple instruments, *Deep Sea Res., Part I*, *44*(11), 1739–1767, doi:10.1016/S0967-0637(97)00029-0.

Jackson, G. A., A. M. Waite, and P. W. Boyd (2005), Role of algal aggregation in vertical carbon export during SOIREE and in other low biomass environments, *Geophys. Res. Lett.*, *32*, L13607, doi:10.1029/2005GL023180.

Juul-Pedersen, T., T. G. Nielsen, C. Michel, E. F. Møller, P. Tiselius, P. Thor, M. Olesen, E. Selander, and S. Gooding (2006), Sedimentation following the spring bloom in Disko Bay, West Greenland, with special emphasis on the role of copepods, *Mar. Ecol. Prog. Ser.*, *314*, 239–255, doi:10.3354/meps314239.

Kiørboe, T., and J. L. S. Hansen (1993), Phytoplankton aggregate formation: Observations of patterns and mechanisms of cell sticking and the significance of exopolymeric material, *J. Plankton Res.*, *15*(9), 993–1018, doi:10.1093/plankt/15.9.993.

Kiørboe, T., K. P. Andersen, and H. G. Dam (1990), Coagulation efficiency and aggregate formation in marine phytoplankton, *Mar. Biol.*, *107*(2), 235–245, doi:10.1007/BF01319822.

Lampitt, R. S., W. R. Hillier, and P. G. Challenor (1993), Seasonal and diel variation in the open ocean concentration of marine snow aggregates, *Nature*, *362*(6422), 737–739, doi:10.1038/362737a0.

Legendre, L., and R. B. Rivkin (2002), Fluxes of carbon in the upper ocean: Regulation by food-web control nodes, *Mar. Ecol. Prog. Ser.*, *242*, 95–109, doi:10.3354/meps242095.

Li, W. K. W., F. A. McLaughlin, C. Lovejoy, and E. C. Carmack (2009), Smallest algae thrive As the Arctic Ocean Freshens, *Science*, *326*(5952), 539, doi:10.1126/science.1179798.

Loeng, H. (1991), Features of the physical oceanographic conditions of the Barents Sea, *Polar Res.*, *10*(1), 5–18, doi:10.1111/j.1751-8369.1991.tb00630.x.

Loeng, H., V. Ozhigin, and B. Ådlandsvik (1997), Water fluxes through the Barents Sea, *ICES J. Mar. Sci.*, *54*, 310–317, doi:10.1006/jmsc.1996.0165.

Lundsgaard, C., M. Olesena, M. Reigstad, and K. Olli (1999), Sources of settling material: Aggregation and zooplankton mediated fluxes in the Gulf of Riga, *J. Mar. Syst.*, *23*, 197–210, doi:10.1016/S0924-7963(99)00058-5.

McCave, I. N. (1984), Size spectra and aggregation of suspended particles in the deep ocean, *Deep Sea Res., Part A*, *31*(4), 329–352, doi:10.1016/0198-0149(84)90088-8.
McDonnell, A. M. P., and K. O. Buesseler (2010), Variability in the average sinking velocity of marine particles, *Limnol. Oceanogr.*, *55*(5), 2085–2096, doi:10.4319/lo.2010.55.5.2085.
Møller, E. F., T. G. Nielsen, and K. Richardson (2006), The zooplankton community in the Greenland Sea: Composition and role in carbon turnover, *Deep Sea Res., Part I*, *53*(1), 76–93, doi:10.1016/j.dsr.2005.09.007.
Möller, K. O., M. St John, A. Temming, J. Floeter, A. F. Sell, J. P. Herrmann, and C. Möllmann (2012), Marine snow, zooplankton and thin layers: Indications of a trophic link from small-scale sampling with the Video Plankton Recorder, *Mar. Ecol. Prog. Ser.*, *468*, 57–69, doi:10.3354/meps09984.
Morán, X. A. G., Á. López-Urrutia, A. Calvo-Díaz, and W. K. W. Li (2010), Increasing importance of small phytoplankton in a warmer ocean, *Global Change Biol.*, *16*(3), 1137–1144, doi:10.1111/j.1365-2486.2009.01960.x.
Moum, J. N. (1996), Efficiency of mixing in the main thermocline, *J. Geophys. Res.*, *101*(C5), 12,057–12,069, doi:10.1029/96JC00508.
Olli, K., C. W. Rieser, P. Wassmann, T. Ratkova, E. Arashkevich, and A. Pasternak (2002), Seasonal variation in vertical flux of biogenic matter in the marginal ice zone and the central Barents Sea, *J. Mar. Syst.*, *38*, 189–204, doi:10.1016/S0924-7963(02)00177-X.
Osborn, T. R. (1980), Estimates of the local rate of vertical diffusion from dissipation measurements, *J. Phys. Oceanogr.*, *10*(1), 83–89, doi:10.1175/1520-0485(1980)010<0083:EOTLRO>2.0.CO;2.
Passow, U., and P. Wassmann (1994), On the trophic fate of *Phaeocystis pouchetii* (Hariot): IV. The formation of marine snow by *P. pouchetii*, *Mar. Ecol. Prog. Ser.*, *104*, 153–161.
Prairie, J. C., K. Ziervogel, C. Arnosti, R. Camassa, C. Falcon, S. Khatri, R. M. McLaughlin, B. L. White, and S. Yu (2013), Delayed settling of marine snow at sharp density transitions driven by fluid entrainment and diffusion-limited retention, *Mar. Ecol. Prog. Ser.*, *487*, 185–200, doi:10.3354/meps10387.
Prandke, H., and A. Stips (1998), Test measurements with an operational microstructure-turbulence profiler: Detection limit of dissipation rates, *Aquat. Sci.*, *60*(3), 191–209, doi:10.1007/s000270050036.
Reigstad, M., and P. Wassmann (2007), Does *Phaeocystis* spp. contribute significantly to vertical export of organic carbon?, *Biogeochemistry*, *83*(1–3), 217–234, doi:10.1007/s10533-007-9093-3.
Reigstad, M., C. Wexels Riser, and C. Svensen (2005), Fate of copepod faecal pellets and the role of *Oithona* spp., *Mar. Ecol. Prog. Ser.*, *304*, 265–270, doi:10.3354/meps304265.
Reigstad, M., C. W. Riser, P. Wassmann, and T. Ratkova (2008), Vertical export of particulate organic carbon: Attenuation, composition and loss rates in the northern Barents Sea, *Deep Sea Res., Part II*, *55*, 2308–2319, doi:10.1016/j.dsr2.2008.05.007.
Richardson, T. L., and G. A. Jackson (2007), Small phytoplankton and carbon export from the surface ocean, *Science*, *315*(5813), 838–840, doi:10.1126/science.1133471.
Riebesell, U. (1991), Particle aggregation during a diatom bloom. 2. Biological aspects, *Mar. Ecol. Prog. Ser.*, *69*(3), 281–291, doi:10.3354/meps069281.
Riebesell, U., M. Reigstad, P. Wassmann, T. Noji, and U. Passow (1995), On the trophic fate of *Phaeocystis pouchetii* (Harlot): VI. Significance of *Phaeocystis*-derived mucus for vertical flux, *Neth. J. Sea Res.*, *33*(2), 193–203, doi:10.1016/0077-7579(95)90006-3.
Schindelin, J., et al. (2012), Fiji: An open-source platform for biological-image analysis, *Nat. Methods*, *9*(7), 676–682, doi:10.1038/nmeth.2019.
Slagstad, D., and K. Støle-Hansen (1991), Dynamics of plankton growth in the Barents Sea: Model studies, *Polar Res.*, *10*(1), 173–186, doi:10.1111/j.1751-8369.1991.tb00643.x.
Smayda, T. J. (1970), The suspension and sinking of phytoplankton in the sea, *Oceanogr. Mar. Biol.*, *8*, 353–414.
Smetacek, V. S. (1985), Role of sinking in diatom life-history cycles—Ecological, evolutionary and geological significance, *Mar. Biol.*, *84*(3), 239–251, doi:10.1007/bf00392493.
Sundfjord, A., I. Fer, Y. Kasajima, and H. Svendsen (2007), Observations of turbulent mixing and hydrography in the marginal ice zone of the Barents Sea, *J. Geophys. Res.*, *112*, C05008, doi:10.1029/2006JC003524.
Svensen, C., C. Wexels Riser, M. Reigstad, and L. Seuthe (2012), Degradation of copepod faecal pellets in the upper layer: Role of microbial community and *Calanus finmarchicus*, *Mar. Ecol. Prog. Ser.*, *462*, 39–49, doi:10.3354/meps09808.
Tamigneaux, E., L. Legendre, B. Klein, and M. Mingelbier (1999), Seasonal dynamics and potential fate of size-fractionated phytoplankton in a temperate nearshore environment (Western Gulf of St Lawrence, Canada), *Estuarine Coastal Shelf Sci.*, *48*(2), 253–269, doi:10.1006/ecss.1999.0416.
Thévenaz, P., and M. Unser (2007), User-friendly semiautomated assembly of accurate image mosaics in microscopy, *Microsc. Res. Technol.*, *70*(2), 135–146, doi:10.1002/jemt.20393.
Utermöhl, v. H. (1931), Neue Wege in der quantitativen Erfassung des Planktons. (Mit besondere Berücksichtigung des Ultraplanktons), *Verh. Int. Verein. Theor. Angew. Limnol.*, *5*, 567–595.
Våge, S. (2010), Structure and dynamics of the Barents Sea Polar Front near the Great Bank and associated plankton distribution in August 2007, MS thesis, Dep. of Arctic and Mar. Biol., Univ. of Tromsø, Tromsø, Norway.
Wassmann, P. (1998), Retention versus export food chains: Processes controlling sinking loss from marine pelagic ecosystems, *Hydrobiologia*, *363*, 29–57, doi:10.1023/A:1003113403096.
Wassmann, P., R. Peinert, and V. Smetacek (1991), Patterns of production and sedimentation in the boreal and polar Northeast Atlantic, *Polar Res.*, *10*(1), 209–228, doi:10.1111/j.1751-8369.1991.tb00647.x.
Wexels Riser, C., P. Wassmann, K. Olli, A. Pasternak, and E. Arashkevich (2002), Seasonal variation in production, retention and export of zooplankton faecal pellets in the marginal ice zone and central Barents Sea, *J. Mar. Syst.*, *38*, 175–188, doi:10.1016/s0924-7963(02)00176-8.
Wexels Riser, C., M. Reigstad, P. Wassmann, E. Arashkevich, and S. Falk-Petersen (2007), Export or retention? Copepod abundance, faecal pellet production and vertical flux in the marginal ice zone through snap shots from the northern Barents Sea, *Polar Biol.*, *30*(6), 719–730, doi:10.1007/s00300-006-0229-z.
Yamazaki, H., and T. Osborn (1990), Dissipation estimates for stratified turbulence, *J. Geophys. Res.*, *95*(C6), 9739–9744, doi:10.1029/JC095iC06p09739.